Experiments in Superconductivity: The Meissner and Josephson Effects

Edwin Ng*
MIT Department of Physics
(Dated: April 9, 2012)

We perform a series of basic experiments in superconductivity on vanadium, lead and niobium bulk samples using liquid helium cryogenics. We measure T_c for each sample via the Meissner effect and demonstrate for vanadium a dependence of T_c on an external B field. We observe the presence of persistent currents by measuring the trapped flux in a superconducting lead cylinder. Finally, we observe the DC Josephson effect through a Nb-Al_2O_3-Nb junction, and we measure the critical current as a function of an external B field to determine the fundamental flux quantum, which we find to be $(1.93 \pm 0.01_{\text{stat.}} \pm 0.1_{\text{syst.}}) \times 10^{-7}$ G cm^2.

I. INTRODUCTION AND THEORY[1]

Superconductivity (SC) is a phenomenon which occurs in various materials at low temperatures, including thirty elements and thousands of compounds. One aspect of superconductivity is zero resistance; in this sense, a superconductor is similar to a perfect classical conductor. However, superconductors also exhibit other distinctive properties. In this lab, we study the Meissner effect, the hallmark of SC, as well as the Josephson effect, which has important applications to high-precision measurements.

Superconductivity occurs only under certain conditions. In the absence of an external magnetic B field, there is a critical temperature T_c below which the material becomes superconducting. When $B \neq 0$, however, the transition temperature is lowered; empirically, the condition for SC is

$$B \leq B_0 \left[1 - \left(\frac{T}{T_c}\right)^2\right], \tag{1}$$

where B_0 is the field above which SC cannot occur, even at $T \to 0$. Thus, we can think of the transition to SC as a phase transition in B and T, with the SC phase delimited according to Equation 1.

This condition and other properties of superconductors, such as heat capacities, can be derived with BCS theory, formulated by Bardeen, Cooper, and Schrieffer in 1957. In BCS theory, electrons at low temperatures couple to form Cooper pairs via vibrations of the lattice. These Cooper pairs then condense into a ground state, where they flow freely without resistance.

There is also a distinction between the so-called Type I and Type II superconductors. Type I superconductors include most of the elemental superconductors and are characterized by a sharp transition at T_c. Type II superconductors, on the other hand, develop non-SC vortices near T_c, resulting in a mixture of SC and non-SC properties during the transition; they are therefore characterized by wider transitions and more persistent SC behavior around T_c.[2] Of the samples we use, lead is a Type I SC while vanadium and niobium are Type II.

* ngedwin@mit.edu

I.1. The Meissner Effect

The Meissner effect sets superconductors apart from perfect classical conductors. Generally speaking, the Meissner effect is the empirical observation, made by F.W. Meissner in 1933, that superconductors exclude magnetic fields from their interior. The London equations, proposed by Fritz and Heinz London in 1935, give a phenomenological account for this effect.

More specifically, the London equations show that a superconductor obeys $B_{\text{sc}} = Be^{-z/\lambda_L}$, where B is the external field, z is the depth from the surface of the SC, and λ_L is the material-dependent London penetration depth. Thus, magnetic fields can exist only at the surface of the SC; for depths z larger than λ_L, B_{sc} is effectively zero. We can therefore also view superconductors as exhibiting perfect diamagnetism.

Physically, this effect is achieved through the presence of surface currents. These surface currents act to precisely cancel out the field in the interior of the SC, thus bringing about the Meissner effect. In this lab, we take advantage of this flux exclusion to detect the transition into SC, which allows us to determine T_c.

Moreover, since superconductors also have zero resistence, these surface currents can potentially be persistent. That is, once these surface currents are set up, they can be made to flow indefinitely, as long as the sample remains below T_c and the $B = 0$ condition is respected.

I.2. The Josephson Effect

The Josephson effect involves the tunneling of the Cooper pairs across a narrow insulating gap, called a Josephson junction, and is named after B.D. Josephson for his discovery of it in 1962.

We consider the application of a DC voltage V_0 across two superconductors separated by a narrow insulating gap. Because the electrons are bound into Cooper pairs, there are no free electrons for single-particle tunneling across the junction, and so there should be no resulting current until we exceed the binding energy of the Cooper pairs, upon which we get a nonlinear return to an Ohmic response as the Cooper pairs break up.

Nevertheless, Josephson discovered that when the gap is narrow enough, the two superconductors can still cou-

ple together and result in the tunneling of the Cooper pairs themselves. This Josephson current density is[3]

$$J(t) = J_0 \sin\left(\delta_0 + \frac{1}{\Phi_0} V_0 t\right),$$

where δ_0 is a constant phase, J_0 is the critical current density, and $\Phi_0 = h/2e$ is the flux quantum.

Thus, when $V_0 = 0$, we get a finite and constant Josephson current, proportional to J_0. On the other hand, when $V_0 \neq 0$, the Josephson current oscillates with high frequency (dictated by $1/\Phi_0$); this current averages out to zero, until V_0 surpasses the binding energy of the Cooper pairs and we return to Ohmic response.

This DC Josephson effect is of particular interest to us because the critical current J_0 is itself related to Φ_0. In particular, if we apply a static magnetic field $\mathbf{B} = B\hat{\mathbf{z}}$ perpendicular to the gap, then the coupling of the superconductors across the junction can be described by[4]

$$g(\mathbf{r}) = g_0 \exp\left(2\pi i \cdot \frac{1}{\Phi_0} \int_C \mathbf{A} \cdot \mathrm{d}\mathbf{r}\right),$$

for g_0 a constant and $\mathbf{B} = \boldsymbol{\nabla} \times \mathbf{A}$ under some gauge choice. The integral is taken over the path C travelled by the Cooper pairs as they cross the gap and is analogous to an Aharonov-Bohm effect. Finally, we can relate this coupling to the measured J_0 by the relation[4]

$$J_0 = \left| \iint_S g(\mathbf{r})\, \mathrm{d}^2\mathbf{r} \right|,$$

where S is the x-y cross-section of the junction.

As described in Section II.3, the setup of our Josephson junction is approximately a cylindrical superconducting wire of radius R split by a cylindrical gap of width D. Hence, we take C to be along the axial direction $\hat{\mathbf{x}}$, S to be the circular x-y cross-section, and $\mathbf{A} = -By\,\hat{\mathbf{x}}$ along the gap and zero elsewhere. If we define $\Phi = (2RD)B$ to be the flux perpendicular to the junction, then

$$J_0 = \frac{2g_0R^2}{\Phi/\Phi_0} \left| \mathcal{J}_1\left(\frac{\pi\Phi}{\Phi_0}\right) \right|, \tag{2}$$

where $\mathcal{J}_n$ denotes the nth Bessel function of the first kind. This is the basic model we will use in determining the fundamental flux quantum.

II. EXPERIMENTAL APPARATUS

We can organize the experiments according to the probes used to perform them. Probe I allows for T_c measurements of our various samples by exploiting the flux exclusion of the Meissner effect. Probe II is dedicated to the observation of persistent currents, and probe III contains the chip used to study the Josephson effect. The following discussion mostly follows that of [1].

Each of the probes consists of a long hollow metal tube which ends in a head containing the sample and the necessary apparatus. This head is lowered through the neck of a standard 30 L liquid helium dewar and kept in place by a lock collar. Circuitry extends out of the tube to connecting ports on the top. Detailed pictures can be found in [1], and we discuss the essential components and logic of each probe in the following subsections.

Temperature control for probes I and II is achieved by pumping helium out through the probe neck—we control the temperature by adjusting the airflow speed and the depth of the probe head. We typically pump with dewar pressures down to −500 mbar. Probe III does not use pumping, and temperature is controlled by lowering or raising the probe. Temperature readouts vary by probes; we use a calibrated silicon diode for probe I, a carbon resistor for probe II, and a digital readout for probe III.

II.1. Probe I: Measurements of T_c

The head of probe I consists of an outer driving solenoid with 2200 turns, length 31.0 mm, inner diameter 14.0 mm, and outer diameter 16.9 mm. Inside this solenoid is a test-coil solenoid consisting of 810 turns, length 12.0 mm, inner diameter 7.1 mm, and outer diameter 10.5 mm. The sample is inserted into the inner coil and kept in place with a brass spacer fastened with a threaded loop of wire.

We then drive an AC voltage across the outer solenoid using an Agilent function generator, set to 200 Hz at approximately 500 $\mathrm{mV_{rms}}$. This causes the inner coil to pick up an induced EMF V_C. When the sample transitions from non-SC to SC, the excluded field due to the Meissner effect causes the flux within the inner coil to drop dramatically. Observing the variation of V_C against temperature gives us essentially the SC transition curve.

We measure the RMS value of V_C using a 6-½ digit Agilent multimeter. Typical RMS values for V_C are about 3 mV, although this depends on the function generator voltage. However, upon transitioning to the SC phase, this value usually drops by 1 mV for the type II (V and Nb) samples, and by about 0.2 mV for the type I Pb sample (following a gradual decline of about 0.5 mV due to the conductivity of Pb at low but non-SC temperatures).

Temperature readout is made by a silicon diode situated 1 cm above the sample, calibrated in [1] with a 10 µA, 9 V battery source. The calibrated diode response ranges from about 0.5 V at 300 K to about 1.7 V at 1.4 K. The diode voltage V_T is monitored by a second 6-½ digit Agilent multimeter. In order to make more faithful measurements of the crucial sample temperature, we also add a small spring between the spacer and the sample, to ensure its proximity to the diode.

In addition to measuring T_c of each sample, we can also observe the trend predicted by Equation 1 for our vanadium sample, by applying a DC component to the outer solenoid voltage. This is done by connecting an HP DC power supply in parallel with the function generator, and putting a Fluke digital multimeter in series to monitor the current. Since the loading changes, we adjust the function generator to about 850 $\mathrm{mV_{rms}}$.

II.2. Probe II: Persistent Currents

The head of probe II contains a single driving solenoid, consisting of 2210 turns, a length of 44.5 mm, and an inner diameter of 14.3 mm. Inside this solenoid is a lead cylinder, with an outer diameter of 14.0 mm, an inner diameter of 11.0 mm, and a length of 90 mm.

The solenoid is fed a DC current (about 100 mA) by an HP DC power supply, monitored with a Fluke multimeter. Temperature readout is made using an (uncalibrated) carbon resistor, which reads about 300 Ω at room temperature and up to 2800 Ω near 4.2 K. We pass a 10 µA current through the resistor to read off the voltage V_R using the Agilent multimeter.

To measure the magnetic field B within the lead cylinder, we use a Hall probe. The probe is fed a current of 35 mA by a Hall probe box, which also outputs the Hall voltage V_H (read by the Agilent multimeter) and contains a bias control for calibration.

Here, the idea is to subject the lead cylinder to an external static field while it is non-SC, and then cool it below T_c. At this point, surface currents develop on both the inner and outer surfaces of the cylinder, to keep the field in the material zero and B elsewhere.

We then turn off the external field, which will cause the outer surface currents to disappear but preseve the inner surface currents, which flow without resistance. Thus, even though the external field is zero, the Hall probe reads a nonzero field within the cylinder due to the trapped flux. We can then raise the temperature of the sample until it again becomes non-SC, upon which we expect to see V_H drop to zero, indicated the quenching of the inner surface currents.

II.3. Probe III: Josephson Junction

Probe III contains a chip provided by Lincoln Labs and Prof. T. Orlando, containing 81 Nb-Al_2O_3-Nb junctions, of which this setup will use one. The superconducting niobium is shaped as a cylindrical wire with a diameter of $2R = 15$ µm and a thickness D of 1.5–2.0 nm.

Temperature readout is provided digitally and no adjustments or calibrations are necessary. Furthermore, we are given[1] that the London penetration depth for Niobium at $T_c = 9.2$ K is approximately 39 nm, which we must add to the insulating gap, along with a correction factor of $1/\sqrt{1-(T/T_c)^4}$ when at temperature $T < T_c$.

A switching box is provided that takes in the driving voltage along ports I_+/I_- and outputs the response of the junction via V_+/V_-, each with resistance 1 kΩ. We attach a function generator to I_+/I_- to sweep the driving voltage, at 200 Hz and 1.5 V_{pp}; compared to the characteristic DC Josephson oscillation frequency of[1] 484 MHz/µV, this is essentially an extremely slowly-varying driving voltage, and we safely treat it as DC. We furthermore tee the output of the function generator to CH2 of a Rigol oscilloscope, set to averaging and XY mode in order to view the I-V curve of the junction.

Next, to get the response, we take the output of the V_+/V_- ports and feed it into a Stanford Research preamplifier, set to DC coupling $A-B$ and 100 gain. We feed its output on 50 Ω to CH1 on the oscilloscope.

We also want to be able to apply a static external B field to the junction, in order to measure the flux quantum. Around the junction, we have a solenoid consisting of 2000 turns of 36 AWG magnet wire around a brass cylinder, designed to produce a field of 540 G/A perpendicular to the axis of the junction. We use the DC current supply and monitor the current with the Fluke multimeter, taking care not to exceed 200 mA of current, and reduce the driving voltage to 410 mV_{pp}.

III. PROCEDURE AND OBSERVATIONS

III.1. Probe I

Once the transition is approximately found by pumping, we alternately cool and warm the sample through T_c, and record the readout for V_C and V_T by filming the multimeters using an iPhone camera, for later processing. Generally, for each sample, we obtain three to four iterations of cool down and warm up, in order to establish consistency and observe the effects of hysteresis. In our analysis, we then pick a representative video to sample.

In order to determine the T_c dependence on B in vanadium, we use the setup described in Section II.1 and use the DC current values {0 mA, 200 mA, 250 mA, 300 mA}. Note that 100 mA data has also been taken, but we later discovered that we have only two videos at that field; combined with the fact that the data point deviates strongly from the trend, we have discarded it.

Figure 1 also shows another indication of the Meissner effect in the lead sample. Using a simple integrator circuit described in [1], we integrate the EMF of the test coil and send the output to an Rigol oscilloscope. Upon transitioning between SC and non-SC, the transient EMF induced by the surface currents leads to a sharp spike in the output, which we can detect with the scope. In addition to the sudden drop in V_C in terms of numbers, this provides also a nice visualization of the Meissner effect.

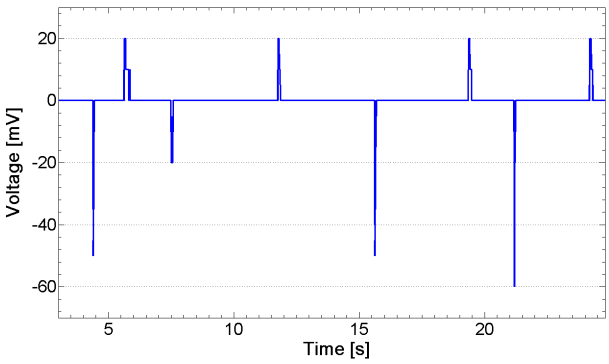

FIG. 1. The transient EMF due to the Meissner effect flux exclusion in lead. The negative spikes are transitions from SC to non-SC, and vice-versa for the positive.

III.2. Probe II

We begin by lowering the probe into the dewar and waiting until we reach 1450 Ω on the resistor, at which point we switch on the Hall probe box, set the current to 35 mA, and adjust the bias so that $V_H = 0$ at $B = 0$.

Next, we perform a calibration of the Hall voltage against an applied field, picking values between 0 mA and 110 mA and measuring V_H. We observe a very linear behavior, and we conclude that the Hall probe response is $(8.201 \pm 0.008) \times 10^{-3}$ V/A.

Finally, we set the applied current to 99.9 mA and lower the temperature further by pumping. In the non-SC phase, we measure $V_H = (0.817 \pm 0.001)$ mV, and between 2070 Ω and 2200 Ω on the carbon resistor, the flux changes slightly to settle at 0.710 mV, indicating the transition to SC.

At this point, we continue to cool the lead cylinder down to about 2500 Ω, at which point we turn $B = 0$, setting the applied current to zero. We observe that V_H remains 0.710 mV, indicating the presence of persistent currents on the inside surface of the cylinder, trapping flux which the Hall probe continues to detect.

Finally, we warm the probe in order to observe quenching of the persistent currents upon the transition to non-SC. In the warming process, V_H gradually increaes to a maximum of 0.716 mV, before sharply falling to 0.007 mV between 1980 Ω and 1600 Ω.

III.3. Probe III

On probe III, we observe an Ohmic linear trace at temperatures above SC for niobium. Around 10 K, we begin to see nonlinearity and the full curve, as shown in Figure 2, shows up clearly around 8 K.

We make several measurements using the scope cursors of the various features, including the critical current J_0 (up to a constant proportionality due to phase), and the voltage corresponding to the binding energy of the Cooper pairs, marked by the sudden rise to Ohmic behavior at high driving voltages. These specific features are labelled in Figure 2.

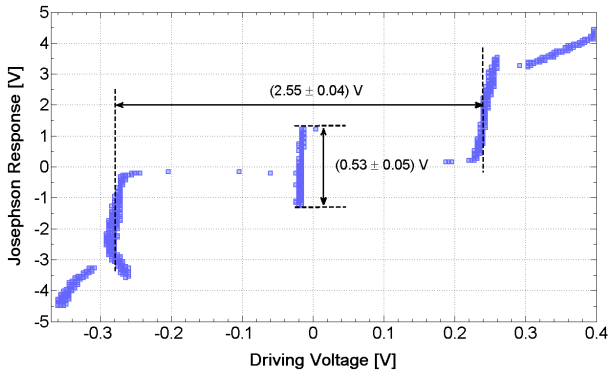

FIG. 2. An I-V curve of the Josephson junction taken at zero applied field with 1.5 V_{pp} driving voltage and at 7.7 K. Note the unexplained bend in the negative quandrant trace.

Next, we connect the DC current supply to the solenoid in order to apply a B field to the gap. First, we vary the current to obtain the shape of the main mode, followed by the second mode, measuring the critical current and its uncertainty using the scope cursors. We observe zeros in the ranges 27.63–30.00mA and 46.44–59.00mA.

To obtain the other half and to determine to horizontal shift in the flux due to the Earth's field, we switch the polarity on the DC supply repeat the process. We observe zeros in the ranges 22.20–25.96mA and 42.8–49.5mA.

IV. DATA REDUCTION AND ANALYSIS

IV.1. Determination of T_c

From each of our T_c measurements, we pick a representative video and sample frames from that video, transferring the extracted numbers to text data. Typical sampling rates are approximately every 5–10 frames, focusing on the transition region.

Once sampled, the text data is plotted in a scatter plot similar to the one in Figure 3. We first delineate the observed transition range and compute the means V_1 and V_2 of the two constant regions, defining their average V_0 to be the test-coil voltage at transition.

Next, we perform a linear fit $y = ax + b$ on the transition range, using a least-squares regression without uncertainties. We define $T_c = (V_0 - b)/a$ to be the critical temperature of the transition. However, since we do not have uncertainties on the fit parameters, we define $E = \sqrt{\sum_i (y - y_i)^2 / N}$ as an "RMS"-like measure of the transition line width, where the sum is taken over those N data points and y refers to the value of the fit at x_i.

We then project this linewidth into the horizontal direction and define the uncertainty in T_c due to the transition line width to be E/a. Since $\delta V_0 \ll E/a$ in general, we have $\delta T_c = E/a$. This process is carried out and presented in Figure 3.

Proceeding in this way, we can obtain estimates on T_c for each sample, which are summarized and calibrated in Table IV.1.

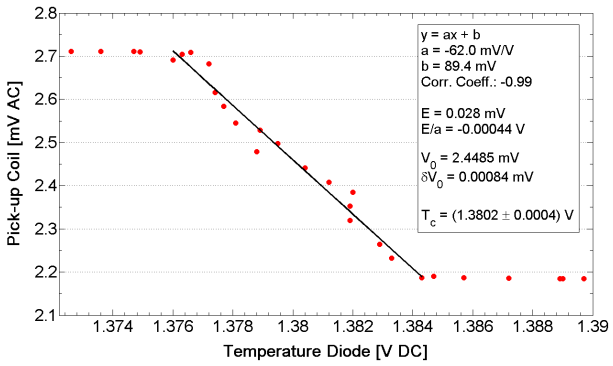

FIG. 3. A sample fit to obtain T_c, in this case for a niobium warm-up video, also serving as an example of a typical transition curve. Intermediate error calculations are shown for reference.

Sample	T_c (K)	Cool Down (K)	Warm Up (K)	Error (K)
V	5.38	6.072 ± 0.009	6.043 ± 0.008	0.66
Pb	7.19	7.787 ± 0.004	7.779 ± 0.004	0.59
Nb	9.46	11.94 ± 0.03	11.50 ± 0.02	2.04

TABLE I. A summary of the determined T_c values for each sample, compared to the published values (second column).[2] The errors are calculated as the discrepancy between the lower of the two values (i.e., warm up) and the published values.

We note that the measured values for T_c seem to be all systematically higher than the published values. One explanation is that the diode calibration contains an offset. J. Steeger has recently determined the diode to read $V_T = (1.6125 \pm 0.0002)\,\mathrm{V}$ at 4.2 K, corresponding to an offset of approximately 0.4 K. It is not known how this offset behaves as a function of V_T, but we do know that the diode is correct at 77 K and room temperature. Judging from niobium, we also believe that pumping speed and a strong temperature gradient between the diode and the sample is responsible.

IV.2. Dependence of T_c on B

We can also carry out the exact same process for each of the data sets for vanadium under varying magnetic fields. Because of the slight discrepancy between the cool down and warm up data sets due to hysteresis and other effects, we decide to plot their average, as shown in Figure 4.

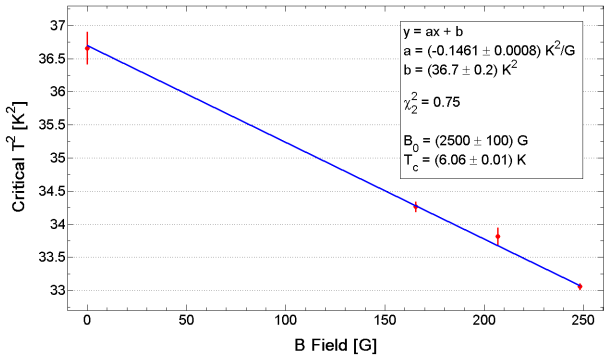

FIG. 4. A linear fit to Equation 1 using averaged vanadium T_c measurements with nonzero external B fields. Error bars represent both the uncertainty from averaging in addition to one-half the difference between warm and cool values.

The value of B_0 is still high compared to the accepted value of about 1500 G (see [1]). We find that correcting for the finite solenoid of the setup only accounts for a factor of 0.9. However, we can positively note a clear dependence T on B, and the fit suggests that the data agrees with Equation 1.

IV.3. Determination of the Flux Quantum

In fitting to Equation 2, we find that we need to modify a few parameters, due to two effects. The first is a vertical shift due to the Earth's magnetic field, and the second is an overall horizontal offset, due to a yet-unknown cause, although we suspect electronic noise. Thus, the model we fit, as shown in Figure 5, is

$$y = \frac{A}{(x-B)/C}\left|\mathcal{J}_1\left[\frac{\pi(x-B)}{C}\right]\right| + D. \tag{3}$$

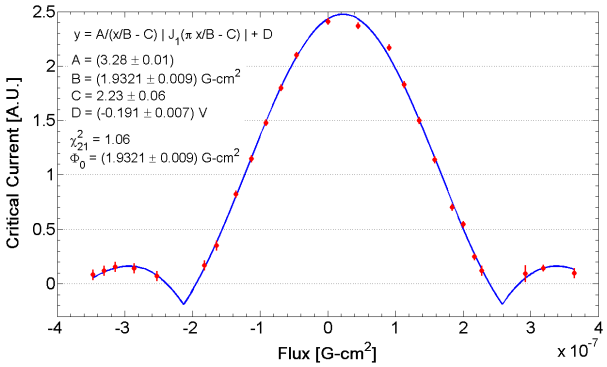

FIG. 5. A nonlinear fit to the Josephson critical current as a function of applied flux using gradient search, according to Equation 3. This data was taken at approximately 7.7 K, so note that a correction factor of 1.4 is necessary to obtain the correct D and Φ.

However, we also know that the correct model is given by Equation 2 and not 3. We therefore have reason to suspect that this leads to a systematic change in our determination of the flux quantum. If we view the horizontal range of the curve below the x-axis as the systematic error, this gives us an uncertainty of about 0.1 G cm^2.

V. CONCLUSIONS

We demonstrate a long series of experiments, unequivocally establishing superconductivity as a physical phenomenon. Despite systematic offsets in determining T_c, most, if not all, of the qualitative features agree with expectations. We furthermore measure the fundamental flux quantum to be $(1.93 \pm 0.01_{\mathrm{stat.}} \pm 0.1_{\mathrm{syst.}}) \times 10^{-7}$ G cm^2, about 7% off from the published value of 2.067×10^{-7} G cm^2.

[1] M.I.T. Junior Lab Staff, "Superconductivity," (2011).
[2] G.S.U. Dept. of Physics, "Hyperphysics - Superconductivity," (2012).
[3] R.P. Feynman, *Feynman Lectures on Physics*, Vol. III (Addison-Wesley, 1965) Chap. 21.
[4] X.-G. Wen, Personal communication (2012).